Mon. Not. R. Astron. Soc. **000**, 000–000 (0000) Printed 3 January 1997 (MN LATEX style file v1.4)

Hotspots on late-type Supergiants.

P.G. Tuthill,[1], C.A. Haniff[2] and J.E. Baldwin[2]
[1]*Space Sciences Laboratory, University of California at Berkeley, Berkeley, California 94720*
[2]*Mullard Radio Astronomy Observatory, Cavendish Laboratory, Madingley Road, Cambridge CB3 OHE*

Accepted 1996 September 18. Received 1996 August 29; in original form 1996 May 24

ABSTRACT

We present the results of a diffraction-limited imaging survey of three nearby M-supergiants using interferometric techniques at the 4.2-m William Herschel Telescope. Between 1992 January and 1993 December all three stars (α Ori, α Sco, and α Her) showed unambiguous evidence at optical wavelengths for asymmetric structures close to, or on, the stellar surface, implying that such features must be a common phenomenon on M-supergiants. Typically these unresolved features, or "hotspots", numbered between one and three, contributed between 5% and 20% of the total flux from the source, and had similar colours to the emission from the stellar disc. The observed timescales for variations of the hotspots were in the range three to nine months, and are thus consistent with a convective origin, as first suggested by Schwarzschild, and with their contributing towards the irregular variability seen in this class of star. The apparent ubiquity of such surface asymmetries implies that the circularly symmetric models often used to interpret high spatial resolution observations of these stars will need to be modified if systematic errors are not to be introduced.

Key words: stars: – imaging – stars: individual: α Ori – stars: individual: α Her – stars: individual: α Sco – stars: supergiants.

1 INTRODUCTION

Ever since the first detection, in February 1989, of a bright unresolved feature on the surface of Betelgeuse (Buscher et al. 1990), the evidence for the continuing presence of "hotspots" on the surface of this late-type supergiant has become increasingly compelling. While the presence of such asymmetries had been suggested by earlier photometric and polarimetric studies (see, for example, Schwarz & Clarke 1984; Hayes 1984), the identification of individual hotspots has relied upon the availability of diffraction-limited imaging, made possible in the main by developments in ground-based interferometry. Images of Betelgeuse obtained in 1991 (Wilson et al. 1992), using the same interferometric non-redundant mask (NRM) techniques as Buscher et al., revealed two hotspots on the stellar disc, and, more recently, Gilliland & Dupree (1996) have detected a bright unresolved feature, offset from the centre of Betelgeuse, in two ultraviolet continuum passbands (2550/236 Å and 2800/316 Å) using the Faint Object Camera of the Hubble Space Telescope. In all of these cases, the stellar brightness distribution could be approximated, at least to first order, by the superposition of a circularly symmetric disc with a small number (≤ 2) of bright unresolved features contributing approximately a few tens of percent of the total flux.

Despite the frequency with which these surface features have been reported – essentially all observational studies sensitive enough to have detected them have detected them – their nature and physical properties have remained unclear. For example, most high-resolution imaging studies of M-supergiants have been exclusively targeted towards Betelgeuse, and so it has not yet been possible to establish whether or not such hotspots are commonplace among stars of similar spectral types. Even for Betelgeuse itself, the absence of an extensive observational database has precluded the determination of either the characteristic lifetimes of the hotspots, or the magnitude of the photometric variability associated with them. Furthermore, there is still no consensus as to the relationship, if any, that exists between the presence of hotspots and the processes that govern the extensive mass loss seen in evolved supergiants.

In this paper we present the results of a multi-epoch optical interferometric study of three nearby M-supergiants: α Ori (Betelgeuse), α Sco (Antares), and α Her (Rasalgethi). In an effort to better characterise the activity first seen on Betelgeuse, all three of these sources were observed on a number of occasions during the period 1992 January–1993 December. Our results represent the first high-resolution imaging survey of this class of star and as such have permitted us to address a number of the issues mentioned above, including the lifetime and behaviour of the surface activity. In the following section we discuss the observations and our methods for data reduction and analysis. In Section 3 we present our results and discuss their implications for models of surface activity, while in Section 4 we summarise our conclusions.

2 OBSERVATIONS, DATA REDUCTION AND ANALYSIS

2.1 Observations

Interferometric observations of α Ori (M1-2 Ia-Iab), α Sco (M1.5 Iab-Ib), and α Her (M5 Ib-II) were obtained at the Ground-based High Resolution Imaging Laboratory of the 4.2-m William Herschel Telescope at several epochs during 1992 and 1993. The sources were chosen primarily on the basis of their expected angular size on the sky, as determined by their magnitudes and colours. In order to optimise the observations for diffraction-limited image recovery, all of the data were collected using the NRM technique described in Buscher et al. (1990). In this method, optics located beyond the nominal telescope focus are used to re-image the telescope pupil onto a mask which selects light from a small number of locations on the primary mirror. These beams are subsequently refocused, at high magnification, onto a fast-readout camera. The effect of the pupil-plane mask is to convert the telescope into an imaging interferometer, with the locations and sizes of the array elements being defined by the transparent portions of the pupil mask. With this arrangement, narrowband short exposure images (interferograms) display a pattern of fringes, the locations and modulations of which encode high-resolution information about the source. Because of the low signal levels associated with the short exposures necessary to freeze the seeing, sequences of many thousands of interferograms are usually recorded to allow improvement of the signal-to-noise via averaging.

For the observations reported here, CCDs with readout noises in the range 5–10 electrons/pixel rms were used as detectors. These were used in a "shutterless" mode with the focal-plane images being squashed on-chip in the vertical direction (i.e. parallel to the interference fringes and perpendicular to the output register) and then read out continually every $10-15$ ms in a 1×256 pixel format. For most of the observations, these exposure times were comparable to, or slightly longer than, the typical atmospheric coherence times of ~ 10 ms. In all cases the aperture masks were linear in design and comprised either four or five approximately r_0-sized sub-apertures matched to the $1'' - 1.5''$ seeing we experienced. This gave interferometer baselines at quasi-uniform intervals from approximately 25 cm to 400 cm. Because of the linear configuration of the masks, data were taken with them aligned at up to nine different position angles on the sky, so as to map out the 2-dimensional structure of each source. At each position angle roughly 5 000 interferograms were recorded through a number of narrowband filters selected to isolate either pseudo-continuum wavelengths (546, 633, 833, and 902 nm) or the TiO molecular band at 710 nm and the nearby pseudo-continuum at 700 nm. In view of the narrow bandwidths of the filters used, no atmospheric dispersion corrector was employed during any of the observations. Depending on the particular target and filter bandpass, photon rates for the observations ranged from approximately ten thousand to four hundred thousand counts per interferogram, corresponding to mean signal levels of between 70 and 3000 counts/pixel/exposure given the 1-d format of the data.

Table 1. Observing log. Calendar dates refer to the start of the night of each observation. The filter wavelengths and bandpasses (FWHM) are given in nm. The final three columns list the number of apertures, the effective aperture diameters (cm) and the maximum baseline (m) for the aperture mask corresponding to each observation.

Object	Date (m/y)	Mean JD -2.44×10^6	Filter $\lambda/\Delta\lambda$	Mask details N_{ap}	Ap. size	B_{max}
α Ori	01/92	8641	700/10	5	19	3.8
	01/92	8641	710/10	5	19	3.8
	01/92	8641	902/50	5	19	3.8
	01/93	8990	700/10	4	28	3.3
	01/93	8991	700/10	5	15	3.7
	01/93	8991	710/10	5	15	3.7
	09/93	9239	633/10	5	16	3.7
	09/93	9238	700/10	5	16	3.7
	12/93	9328	633/10	5	16	3.8
	12/93	9328	700/10	5	16	3.8
α Sco	07/92	8817	700/10	5	15	3.7
	06/93	9148	546/10	5	16	3.8
	06/93	9147	700/10	5	16	3.8
α Her	07/92	8817	633/10	5	15	3.7
	07/92	8815	700/10	5	15	3.7
	07/92	8816	710/10	4	31	3.5
	07/92	8817	710/10	5	15	3.7
	07/92	8817	833/41	5	15	3.7
	06/93	9148	633/10	5	16	3.8
	06/93	9146	700/10	5	16	3.8
	06/93	9147	710/10	5	16	3.8

Observations of each source were interleaved with measurements of unresolved stars at similar locations in the sky. All the observations of α Ori used γ Ori as the calibrator, while for α Sco we used ϵ Sco and β Sco, and for α Her we employed α Oph. Measurements of these stars were used to monitor the atmospheric and instrumental transfer function during the night. The plate scale and orientation of the CCD camera were determined independently each night using interferometric observations of close binary stars with well determined orbits. Typical errors in the plate scale and orientation were of order a few percent and 1 degree respectively. A summary of the observations is given in Table 1.

2.2 Data reduction

The raw short-exposure images were processed using standard methods (Haniff et al. 1987; Buscher et al. 1990) to derive calibrated estimates of the source visibility amplitudes and bispectra. This involved initial correction for the CCD bias level, the sky background, and any bad pixels, and subsequent accumulation of the power spectrum (i.e. visibility amplitude squared) and bispectrum on each baseline and closed loop of baselines sampled by the mask. The mean power spectra and bispectra were then corrected for the effects of photon and readout noise, and finally calibrated using the corresponding quantities as measured from a nearby unresolved star.

Fig. 1 shows a typical pair of power spectra measured

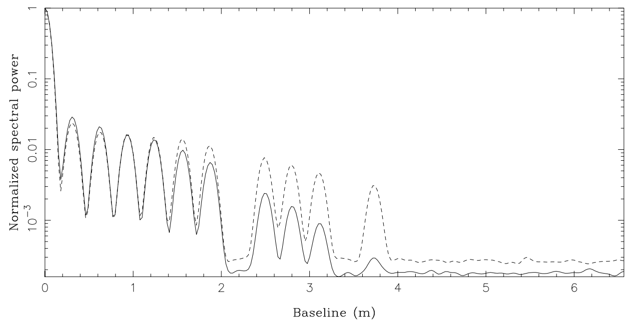

Figure 1. Observed power spectra for α Her (solid line) and its unresolved calibrator α Oph (dashed line) as measured at 710 nm in 1993 June. The spectra peak at the nominal locations of the 10 baselines sampled by the 5-hole pupil mask. Beyond a baseline of 4 m the background signal arises from a combination of readout and photon noise. The reduction in signal level at the longer baselines for α Her is indicative of the large apparent size of the star, and suggests that the source would be almost completely resolved on baselines in excess of ~ 5 m.

with a 5-hole aperture mask for a target and its unresolved calibrator. The gradual decline seen in the power spectrum of the calibrator is indicative of the effects of the spatial and temporal atmospheric perturbations together with other coherence loss mechanisms such as the non-zero filter bandpass and the CCD pixel size. In this example, the source, α Her, is clearly resolved, with the power at the longer baselines being substantially reduced in comparison to that of the point source calibrator, α Oph. Estimates of the calibrated source visibility amplitudes at the nominal interferometer baselines (located at the peaks in the power spectra) were computed by taking the ratio of the noise-corrected values of the normalised mean source and calibrator power spectra. The square root of this quantity then gave the source visibility. All of the sources were sufficiently bright that the errors on the calibrated visibilities were primarily due to short term variations in the atmospheric transfer function rather than the detected signal levels. The final errors on the calibrated visibilities were typically of order 10% of the observed visibility.

In most instances calibration of the mean source bispectrum phases (i.e. the closure phases) left them virtually unchanged. The calibrator closure phases were always very close to the value of 0° expected for an unresolved source, with typical values of $0° \pm 2°$ for all closure triangles and orientations of the masks. Errors on the source closure phases ranged from less than a degree for bispectrum coordinates corresponding to loops of relatively short baselines (< 1.5 m), to as much as 20° for closure triangles including longer baselines on which the sources were resolved.

2.3 Data analysis

Once calibrated visibility amplitudes and closure phases had been recovered for each source, further analysis proceeded in two stages. Initially, diffraction-limited images were recovered from the Fourier data using radio-astronomical self-calibration methods (Pearson & Readhead 1984). Because of the use of a non-redundant mask, the calibrated Fourier data corresponded in form very closely to those from a phase-incoherent radio array, and so it was straightforward to use conventional radio astronomical software to recover true images from the measurements. We used a MEM-based self-calibration software package to reconstruct the images, examples of which are shown in Fig. 2. These images are by no means atypical, and show very clearly the level of asymmetric structure visible in the stellar brightness distributions at differing epochs.

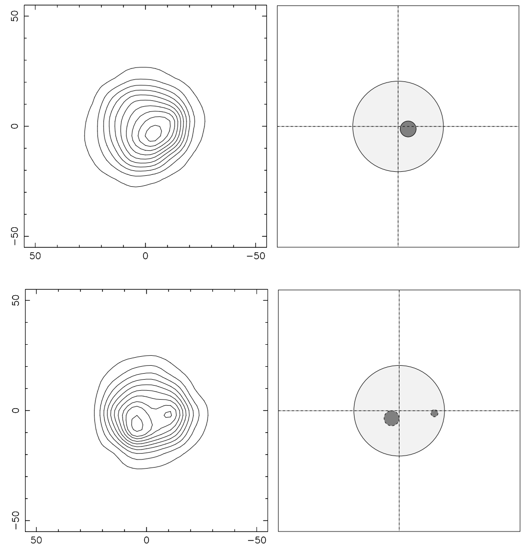

Figure 2. Diffraction-limited image reconstructions of α Her at 633 nm obtained in 1992 July (top) and 1993 June (bottom). These were recovered from the Fourier measurements using an MEM-based self-calibration algorithm. Each image can be represented as the superposition of a uniform disc together with a number of unresolved hotspots. For each image, the right-hand panel shows the locations of the model components, the relative flux of each hotspot being represented by its angular diameter. The contour levels are plotted from 5% to 95% of the peak flux, at intervals of 10%. North is to the top and East to the left. The map scales are in milliarcseconds.

Although the image reconstructions were useful for gaining a qualitative insight into the overall structure of each source, quantitative estimates of the varying contributions to the total brightness distribution were obtained by model-fitting to the calibrated Fourier data. In general, the visibility amplitudes of the sources exhibited smooth variations as a function of position angle on the sky, for example as displayed in Fig. 3. This shows the visibility amplitudes and closure phases measured at 633 nm for α Her in 1993 June (i.e. the data used in reconstructing the bottom left-hand image shown in Fig. 2). The reduction of visibility amplitude with baseline length shows that the source is significantly resolved but, more interestingly, the regular modulation of visibility amplitude with PA, on all baselines, indicates a lack of circular symmetry, and implies that the source has its maximum apparent extent when the interferometer baselines are aligned along PA $\sim 100°$.

In the presence of visibility amplitude data alone, we would not have been able to distinguish between centro-

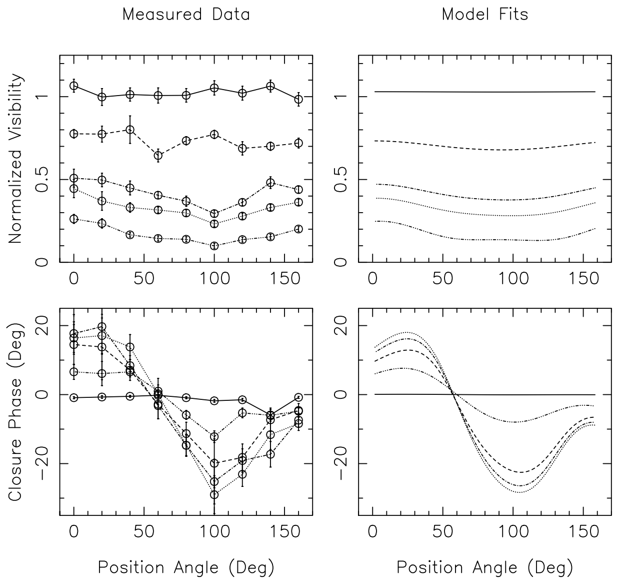

Figure 3. Calibrated visibility amplitudes and closure phases as obtained for α Her at 633 nm in 1993 June. The left-hand panels show the measured data, and the right-hand panels the fits for a model composed of a uniform disc together with two unresolved hotspots on the stellar surface. For clarity, only data corresponding to 5 of the interferometer baselines and 5 of the closure triangles are shown. In these, and subsequent plots, lower azimuthally averaged visibilities correspond to longer interferometer baselines. One-sigma error bars are plotted. For a symmetric source all the closure phases should be zero.

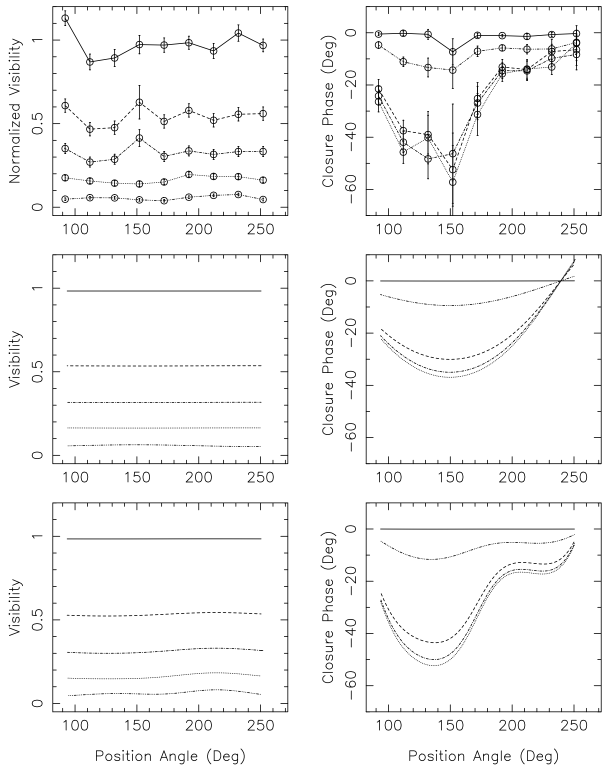

Figure 4. Calibrated visibility amplitudes and closure phases as obtained for α Ori at 700 nm in 1993 December. As in Fig. 3, only data corresponding to 5 of the interferometer baselines and 5 of the closure triangles have been plotted, together with one-sigma error bars. The upper panels show the measured data, while the lower panels show the fits for two different models. The central graphs correspond to the best-fitting uniform-disc plus single spot model, while the lower plots correspond to a model comprising a uniform disc together with two unresolved hotspots.

symmetric but non-circular brightness distributions (e.g. ellipses) and asymmetric source morphologies, as might arise from a uniform disc with a superposed bright feature offset from its centre. However the calibrated closure phases often displayed the unambiguous signature of a non-centrosymmetric source, i.e. the presence of non-zero values (symmetric objects have closure phases of 0° or 180° only). This can be seen quite clearly in the closure phase data for α Her plotted in the bottom left-hand panel of Fig. 3. The closure phases show a smooth variation with position angle, related to the modulation of the visibility amplitudes, and a systematic trend with respect to the baselines involved in any closure triangle: closure triangles involving relatively short baselines show a smaller modulation than those involving baselines on which the source is well resolved. This type of signature, with correlated variations of the visibilities and closure phases, together with regular behaviour of the closure phases as a function of position angle on the sky and type of closure triangle, was seen for essentially all of the targets at all epochs. The only exceptions to this occurred when either the sources were insufficiently resolved or when the data were of low quality. Observations at longer wavelengths (833, 902 nm) suffered from the former of these problems, whereas measurements of Antares, which were always secured at low elevations, tended to fall in the latter category.

In order to characterise the source morphologies quantitatively, we decided to adopt a procedure whereby models of increasing complexity were fit to the measured Fourier data until a satisfactory fit, as measured in a least-squares sense, was obtained. A simple conjugate-gradient algorithm was used to optimise the model parameters, with repeated trials starting from differing initial conditions being used to guard against stagnation in local minima. Based on the image reconstructions, and given the simple functional forms of the visibility measurements, models were constructed from a small number of elements, usually a resolved circularly symmetric component together with a number of unresolved bright features, the locations and magnitudes of which could all be varied. In an effort to estimate the effects of limb-darkening for each star, both uniform-disc and Gaussian functions were used to represent the resolved circularly-symmetric stellar emission. In almost all cases the models incorporating uniform discs were found to give slightly better fits to the data, and so the results of the Gaussian model-fitting are not presented here. In magnetically active stars, including the Sun, large scale magnetic features suppress convection and can give rise to local dark spots on the stellar surface (Baliunas & Dupree 1982). Although the low X-ray fluxes of late-type supergiants (Vaiana et al. 1981) have been interpreted as indicating that their magnetic fields are relatively weak (Belvedere, Chiuderi & Paterno 1982), modelling was also attempted using dark, rather than bright, features superposed on the stellar disc. In all cases, we found that the data could be adequately matched only with the use of a dark-spot model with many more degrees-of-freedom than the corresponding hotspot model. Thus while it was not possible to rule out the presence of dark features on the stellar surfaces, adequate fits were always much more contrived, and so hereafter we shall only refer to the hotspot models.

Some examples of these model-fitting results are presented in Figs. 3 and 4. Fig. 4, in particular, demonstrates the extent to which models of varying levels of complexity were required to provide satisfactory fits to some of the observations. In this figure the model visibility functions shown correspond to uniform discs with one (middle panels) and two (lower panels) superposed hotspots. Although the best-fitting single-spot model reproduces the general trends in the Fourier data, there is a systematic residual, most clearly seen in the closure phase signals. The two-spot model provides a much better fit to the data, matching the excursions in both the visibility amplitudes and closure phases very well.

In summary then, quantitative descriptions of the stellar brightness distributions were derived by fitting parameterised models to the measured visibility amplitudes and closure phases. In view of the numerous possibilities, models were chosen so as to simultaneously satisfy the criteria of (i) simplicity, (ii) consistency with the image reconstructions, and (iii) physical credibility. The full results from the model-fitting are given in Table 2.

3 RESULTS AND DISCUSSION

The basic results of our study are given in Table 2 which shows the best-fit model parameters for each star at each epoch, and for each colour at which the star was observed. Results are presented for the disc-plus-hotspot(s) model with the smallest number of degrees-of-freedom able to fit the data satisfactorily, as well as for a simpler single-component uniform-disc model so as to permit comparison with other measurements in the literature.

3.1 Presence of hotspots

Perhaps the most remarkable feature of Table 2 is the frequency with which asymmetric source structures were detected. In the context of our model parameterisation, hotspots were observed at all epochs for α Ori and α Her, and during one of the two observing runs at which α Sco was targeted. If we include the earlier NRM observations of Betelgeuse by Buscher et al. (1990) and by Wilson et al. (1992), then there seems no doubt that, at least for this source, irregularities must be a common feature of the stellar brightness distribution. Furthermore, our new observations of α Her and α Sco, together with the independent measurements of R Dor by Bedding and co-workers (Bedding, private communication) and the analyses of lunar occultation events for α Sco (see, for example, Evans (1957) and Richichi & Lisi (1990)), suggest that such phenomena may indeed be ubiquitous amongst late-type giants and supergiants.

The failure of many earlier high-resolution imaging studies to reveal these asymmetries is at first sight surprising, but is most likely due to a combination of two factors. In essence, our detections have been based on an analysis of accurate measurements of both the source visibility amplitudes and closure phases, with by far the more important role being played by the latter. Most previous investigations have, however, either relied upon visibility amplitude measurements alone, or have employed methods that have not been as successful in characterising the phase content of the source visibility functions. For example, both Wilson et al. (1992) and Bedding, Robertson & Marson (1994) observed α Sco using NRM methods, but both teams were unsuccessful in measuring its visibility function below a value of $\sim$ 25%, i.e. on exactly those baselines for which the corresponding closure phases would have been expected to be large. Their data are thus not inconsistent with asymmetries being present, at least at the rather moderate level we have seen for α Sco.

3.2 Hotspot parameters

3.2.1 Numbers, locations and relative fluxes

As demonstrated by both Figs. 3 and 4, and Table 2, all our interferometric measurements could be well fit by models composed of at most three unresolved hotspots superposed on an otherwise symmetric disc. This upper limit no doubt reflects the limited extent of the Fourier measurements we were able to secure at each epoch, together with the precision of the individual data themselves, and so higher resolution observations will be necessary to establish whether or not any of the features we have seen correspond to multiple structures on even smaller scales. Nevertheless, a robust conclusion appears to be that quite complicated surface brightness distributions are not uncommon for the three stars in our sample.

The distribution and fluxes of the hotspots were in general well correlated. The brighter features, which always contributed between 12% and 16% of the total flux, were invariably located close to the stellar centre, whereas the secondary spots ($<$ 6%) were most often found closer to the stellar limb. If, as seems likely, the hotspots correspond to features at the deeper photospheric levels, then two explanations for this correlation present themselves. In the first instance, hotspots further from the centre of the disc should be increasingly foreshortened, and so appear less bright to an observer. Second, any obscuration due to the extended cool atmospheres of M-supergiants is expected to be enhanced for features close to the stellar limb. The assumption implicit in both of these arguments is thus that the hotspots have a narrow range of intrinsic flux and that the observed variations in their brightnesses are due to external effects. Future higher sensitivity observations should be able to test this model by measuring the effects of limb darkening and foreshortening, and by possibly detecting the population of fainter features expected towards the stellar limb.

Table 2. Summary of model-fitting results. For each epoch and wavelength, details are given for a simple uniform-disc fit, together with the parameters (diameters, polar co-ordinates, and fluxes) of the simplest uniform-disc plus hotspot model able to satisfactorily characterise the measured data. The stellar diameter and radial co-ordinate of the hotspots (r) are given in milliarcseconds, and θ is measured in degrees North through East. In cases where no hotspot model is listed, the closure phases had values consistent with those of an unresolved source to within the measurement errors. 1-sigma errors are given.

Object	Date	λ	Uniform-Disk			Bright Features		
		nm	Flux (%)	Diam.		Flux (%)	r	θ
α Ori	01/92	700	100	43.5 ± 2.0		-	-	-
			86 ± 10	49 ± 7	(1)	11 ± 6	1 ± 1	$+69^\circ \pm 40^\circ$
					(2)	2 ± 1	16 ± 4	$-54^\circ \pm 10^\circ$
	01/92	710	100	46.3 ± 2.5		-	-	-
			79 ± 6	58 ± 2	(1)	17 ± 2	2 ± 1	$+40^\circ \pm 10^\circ$
					(2)	4 ± 1	29 ± 3	$-45^\circ \pm 5^\circ$
	01/92	902	100	42.6 ± 3.0		-	-	-
	01/93	700	100	43.5 ± 2.0		-	-	-
			79 ± 5	51 ± 4	(1)	18 ± 4	4 ± 3	$+187^\circ \pm 30^\circ$
					(2)	3 ± 2	27 ± 8	$+16^\circ \pm 15^\circ$
	01/93	710	100	45.7 ± 3.0		-	-	-
			71 ± 3	65 ± 4	(1)	23 ± 3	6 ± 2	$+188^\circ \pm 10^\circ$
					(2)	6 ± 4	12 ± 7	$-6^\circ \pm 15^\circ$
	09/93	633	100	54.2 ± 4.0		-	-	-
			82 ± 3	60 ± 2	(1)	12 ± 2	3 ± 1	$-30^\circ \pm 20^\circ$
					(2)	5 ± 1	25 ± 2	$+115^\circ \pm 5^\circ$
					(3)	4 ± 1	21 ± 3	$+68^\circ \pm 10^\circ$
	09/93	700	100	49.3 ± 3.0		-	-	-
			83 ± 3	58 ± 2	(1)	11 ± 2	5 ± 1	$-45^\circ \pm 7^\circ$
					(2)	6 ± 1	10 ± 2	$+91^\circ \pm 7^\circ$
	12/93	633	100	48.6 ± 2.0		-	-	-
			83 ± 2	54 ± 4	(1)	11 ± 3	4 ± 1	$-37^\circ \pm 15^\circ$
					(2)	3 ± 3	5 ± 5	$+174^\circ \pm 60^\circ$
					(3)	2 ± 1	26 ± 5	$+125^\circ \pm 10^\circ$
	12/93	700	100	47.1 ± 2.5		-	-	-
			83 ± 2	54 ± 3	(1)	14 ± 3	3 ± 1	$-29^\circ \pm 10^\circ$
					(2)	2 ± 1	18 ± 6	$+120^\circ \pm 10^\circ$
α Sco	07/92	700	100	33.2 ± 3.0		-	-	-
	06/93	546	100	38.6 ± 4.0		-	-	-
	06/93	700	100	36.7 ± 2.5		-	-	-
			95 ± 5	37 ± 5	(1)	5 ± 3	12 ± 4	$+88^\circ \pm 20^\circ$
α Her	07/92	633	100	37.5 ± 1.8		-	-	-
			85 ± 6	42 ± 4	(1)	15 ± 6	5 ± 3	$-104^\circ \pm 30^\circ$
	07/92	700	100	34.5 ± 2.5		-	-	-
	07/92	710	100	40.1 ± 1.2		-	-	-
			83 ± 4	48 ± 3	(1)	17 ± 5	2 ± 3	$-94^\circ \pm 25^\circ$
	07/92	833	100	36.4 ± 2.5		-	-	-
	06/93	633	100	36.6 ± 1.8		-	-	-
			80 ± 4	40 ± 3	(1)	14 ± 4	4 ± 2	$+146^\circ \pm 25^\circ$
					(2)	6 ± 2	17 ± 4	$-95^\circ \pm 7^\circ$
	06/93	700	100	34.7 ± 1.5		-	-	-
			79 ± 10	39 ± 4	(1)	18 ± 10	3 ± 2	$+220^\circ \pm 25^\circ$
					(2)	3 ± 1	27 ± 6	$-87^\circ \pm 10^\circ$
	06/93	710	100	39.1 ± 1.6		-	-	-
			82 ± 5	43 ± 2	(1)	14 ± 4	3 ± 1	$+170^\circ \pm 25^\circ$
					(2)	4 ± 1	24 ± 4	$-109^\circ \pm 5^\circ$

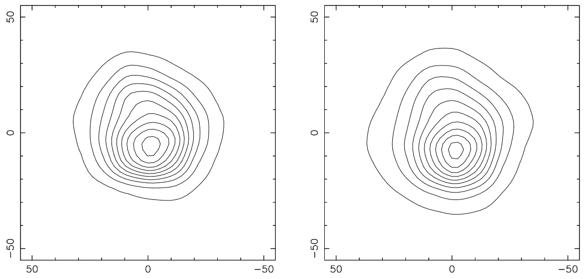

Figure 5. Diffraction-limited image reconstructions of α Ori at 700 nm (left) and 710 nm (right) obtained in 1993 January. Note that, apart from the slightly larger extent of the stellar emission in the TiO band at 710 nm, the images are essentially identical. The availability of multi-colour images allows verification of the imaging and data quality, and additionally shows that the hotspots exhibit relatively little colour dependence. The contour levels are plotted from 5% to 95% of the peak flux, at intervals of 10%. North is to the top and East to the left. The map scales are labelled in milliarcseconds.

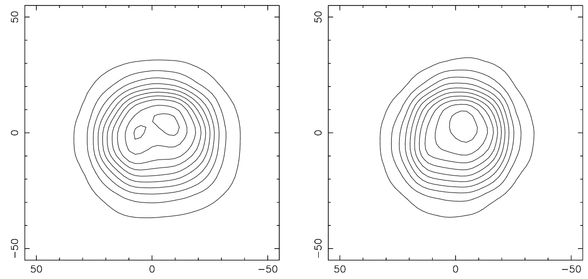

Figure 6. Diffraction-limited image reconstructions of α Ori at 700 nm obtained in 1993 September (left) and 1993 December (right). Note the fading of the secondary south-eastern hotspot, and the relative permanence of the primary hotspot. Contour levels are plotted from 5% to 95% of the peak flux, at intervals of 10%. North is to the top and East to the left. The map scales are labelled in milliarcseconds.

3.2.2 Colours, temperatures and sizes

While the multi-wavelength measurements from most of our observing campaigns span only 250 nm at most, they do suggest that the fractional contribution of any individual hotspot to the total detected flux has only a weak wavelength dependence (see, for example Fig. 5). Our results show a tendency for the fractional hotspot fluxes to be slightly increased in the TiO band (710 nm) as compared to nearby continuum bandpasses, but we believe that this is an artefact due to the enhanced limb-darkening and photospheric extension predicted at this molecular feature (Scholz & Takeda 1987; Bessell et al. 1989).

Evidence for the complicating effects of the wavelength-dependent resolution of our observations is demonstrated by our shorter wavelength (633 nm) measurements of Betelgeuse. These often had sufficiently enhanced resolution, as compared to those at longer wavelengths, to result in more complex closure phase signatures that in turn necessitated more sophisticated modelling. But, despite these differences of detail, the underlying morphologies at varying wavelengths were very similar. Given this instrumental bias, our data are thus not inconsistent with the hypothesis of a wavelength-independent distribution of unresolved hotspots in the stellar brightness distribution.

Because of our limited wavelength baseline, we have been unable to estimate the hotspot temperatures and areas reliably on the basis of the measured relative hotspot fluxes at 633, 700, and 710 nm. However, the image reconstructions and model-fitting both indicate that the bright features cannot have areas much greater than 10% of the stellar disc. In this case, if we assume that they represent regions of higher temperature on the stellar surface, a temperature excess of at least 400 K is required, i.e. a substantial fraction of the median effective temperature of the sample (3450 K). This estimate is consistent with the recent results of Gilliland & Dupree (1996) who interpreted their ultraviolet observations of α Ori in terms of a hotspot with a temperature excess of at least 200 degrees with respect to the underlying stellar disc. While no contemporaneous high-resolution optical images exist for their observation, the agreement between these two independent temperature estimates is reassuring, despite the fact that the optical and ultraviolet data must be probing different layers in the extended stellar atmosphere.

3.2.3 Evolution timescale

One of the most pressing and as yet poorly understood properties of the surface features on M supergiants is their lifetime. The first limit on the evolutionary timescale for these features came from the observations of Buscher and colleagues (Buscher et al. 1990; Wilson et al. 1992). Their images of Betelgeuse, obtained almost two years apart, showed no similarities in their small-scale structure and thus placed an upper limit on the timescale of 23 months. Further studies by Wilson (1992) were able to reduce this limit to 9 months based on observations of Betelgeuse in January and September of 1991. Our new high resolution 633 nm data for α Her show similar rapid changes, with an original hotspot contributing $\sim$ 15% of the flux "transforming" itself into two separate features approximately 15 mas apart on the stellar disc over a period of 11 months.

The measurements reported here for Betelgeuse have allowed us to refine this estimate even further, not least because, for the first time, it has been possible to trace the development of an individual feature over 12 months. This is best demonstrated with reference to Figs. 5 and 6 which together show images of Betelgeuse in the continuum at 700 nm obtained in January, September, and December of 1993. The images from January and September are quite different, with the strongest asymmetric component of the image changing its location from the south to the north hemisphere of the stellar disc. On the other hand, the subsequent variation in the three months from September to December is much smaller. The images from these two months confirm the continuing presence of a prominent bright spot to the north-west of the centre of the stellar disc but reveal a sharp decline in the contribution of a secondary hotspot to the south-east. At all three epochs, independent image reconstructions from data collected at 710 nm exhibited identical behaviour (see Fig. 5), verifying that the evolution seen was intrinsic to the star. Our data thus confirm that even the most dramatic asymmetries can be erased on yearly timescales, and that a characteristic lifetime measured in months is appropriate. It should be stressed, though, that our data only constrain the optical manifestations of the physical phenomena taking place in the stellar atmosphere: the full timescales for the underlying processes may be longer.

3.3 Stellar diameters

The fact that deviations from circular symmetry seem to be both a commonplace and time-variable feature of M-supergiants raises a number of worrying issues regarding previous attempts to measure the apparent sizes of these stars. It is well established that interferometric angular diameter measurements of late-type giants and supergiants show a large scatter (see, for example, Cheng et al. (1986) and Scholz & Takeda (1987)). While this is usually attributed to the use of inadequate representations for the centre-to-limb brightness distribution and the failure to properly treat the strong wavelength-dependant opacity in the cool stellar atmosphere, the results presented here highlight a further problem. If localized features, contributing significantly to the total flux from the source, can appear, evolve in brightness and location, and subsequently disappear, then unless analyses can accommodate such transient events their presence will inevitably introduce systematic sources of error.

This type of model-dependent bias is evident if we compare the uniform-disc diameters determined assuming a centro-symmetric brightness distribution with those inferred using the more complicated models (see Table 2), the latter being systematically higher than the former by between 10 and 20%. Thus, in the context of, for example, effective temperature determinations, the presence of brightness asymmetries would be expected to lead to errors of at least 5–10% in T_{eff} were they not recognized as such. Given the apparently persistent presence of asymmetric structures on the sample stars, we felt it imprudent to use the results of the circularly-symmetric model-fits to investigate the temporal behavior of the stellar diameters. Unfortunately, our results obtained using multi-component models provide relatively poor coverage of the several-hundred day cycles seen in the photometric and radial-velocity measurements of α Ori, α Sco, and α Her (Smith, Patten & Goldberg 1989), and so we have been unable to investigate whether or not our measurements show any evidence for an underlying periodicity in the stellar diameter. Nevertheless, our data for Betelgeuse from 1993 September do imply an anomalously large diameter (~ 59 mas) at that epoch, at which time Betelguese was noticeably fainter than is normal (Krisciunas 1994). Furthermore, data at other epochs did seem to exhibit an anticorrelation with the measured photometric fluxes of Krisciunas. This is certainly consistent with a pulsational model for the photometric variability, but further investigation of this tentative hypothesis will require more frequent observations than reported here. It is interesting to note that Dupree et al. (1987) predict a $\sim 15\%$ variation in the diameter of Betelgeuse if, as they conclude, its photospheric and chromospheric modulation arises from radial pulsation. An effect this large would be straightforward to detect using NRM methods today, particularly as the epoch and period of Betelgeuse's variations are so well defined. We strongly encourage such an observing programme.

Nothwithstanding the effects of surface phenomena, we have compared our uniform disc diameters with previous determinations in the literature. The most recent and useful compilations are those of Dyck et al. (1996) and Richichi & Lisi (1990) who present measurements of all three sample members in the near-infrared, where the effects of limb-darkening and any hotspot signatures are expected to be small. Their combined data give uniform-disc diameters for α Ori, α Sco, and α Her of 44.2 ± 0.2 mas, 41.8 ± 1.0 mas, and 33.0 ± 0.5 mas respectively. If we ignore the anomalous epochs towards the end of 1993, then our uniform-disc fits for α Ori and α Her are in good agreement with these near infrared estimates. There is a somewhat poorer fit for α Sco, but our own results are very similar to the recent optical measurement of Bedding et al. (1994). Their value of 39 ± 3 mas averaged over several wavelength channels between 565 and 582 nm is in good agreement with our 546 nm measurement of 39 ± 4 mas obtained during the better of our two observing runs. This discrepancy between the optical and near-infrared data is consistent with the predictions of limb-darkening calculations (Manduca, Bell & Gustafsson 1977), on the basis of which the measured diameter at 546 nm should have been a factor of 1.1 smaller than the "true" photospheric diameter.

3.4 Physical models

Previous high-resolution studies of M-supergiants, in particular those of Betelgeuse, have suggested a number of possibilities to explain the observed variations in their photometric, radial-velocity and polarimetric signatures. These include the presence of companions, effects due to stellar rotation, magnetic activity, radial and non-radial pulsation, and transient convective cells on the stellar surface. Our new data provide no evidence for the first of these models. The multiplicity of bright features seen on α Ori and α Her together with their irregular evolution on sub-yearly timescales are clearly at odds with the more regular and longer-period behaviour expected for any system of multiple companions. Both α Ori and α Her have been reported to be very close speckle multiple systems (Karovska, Nisenson & Noyes 1986; McAlister et al. 1989), but, to our knowledge, these reports have never been confirmed by independent observers. Our own multi-epoch observations, as well as those of Buscher et al. (1990) and Wilson et al. (1992) showed no evidence for any close stellar companions having magnitude differences with respect to the primaries of less than 4. Thus, although we cannot exclude the possibility that the hotspots are the chaotic manifestation of the regular interaction with nearby faint companions, in the absence of any independent evidence, such an explanation seems unneccesarily contrived.

The irregular and rapid evolution of the spots also argues against a rotational origin. Using angular momentum arguments, Smith et al. (1989) derived a characteristic rotational period for Betelgeuse of approximately 1200 years. Similar physical considerations must also apply to α Her and α Sco, and so, regardless of differences in mass, composition, spectral type, and the details of the angular momentum transport, any rotational timescale will be several orders of magnitude longer than the variability timescales reported here.

As mentioned in Section 2.3, the evidence for strong magnetic activity on late-type supergiants, as determined from their x-ray fluxes, is weak. Limits for the x-ray fluxes of α Ori and α Sco have been reported in the literature (Vaiana et al. 1981; Maggio et al. 1990), but while their total fluxes could be comparable to those of typical late-type dwarfs, their surface fluxes must be very low indeed. Thus, while explanations in terms of local enhancements to the magnetic field that give rise to bright starspots (as opposed to the dark features usually seen on magnetically active stars) remain possible, they are unlikely. Complementary observations together with theoretical predictions for this type of model are clearly required to explore this possibility further.

An argument similar to that ruling out a rotational origin to the brightness asymmetries can also be applied to models invoking radial pulsation. α Ori, α Her, and α Sco all exhibit periodicities in their radial velocities that have been attributed to radial pulsation of the stellar photosphere (Smith et al. 1989). More recently, additional evidence for this model has come via ultraviolet and optical continuum observations of Betelgeuse (Dupree et al. 1990; Smith et al. 1995), which show a regular cycle with a period of ~ 430 days, and optical photometry of α Sco for which a tentative period of 260 days has been reported (Smith et al. 1989). However, while stellar pulsation is likely to be a common feature of late-type supergiants, the more rapid and erratic variability seen in the surface structure of the target stars conflicts with the regularity expected for single mode radial pulsation. Moreover, the observed photometric variability of Betelgeuse, the sample member with the most regular behaviour, is too large (> 0.2 mag) to be explained in terms of the waxing and waning of a small number of hotspots of the type we have detected. One interesting possibility related to radial pulsation has been proposed by Smith et al. (1995). They envisage pulsation in the fundamental mode giving rise to aperiodic shocks that propagate outwards, heating and energizing the extended stellar atmosphere. A natural consequence of this picture is a much more stochastic light-curve, but it remains to be seen whether this type of model can account for the sizes, locations and colours of the features reported here.

Our preferred interpretation for the hotspots is that they represent the observable effects of large convective cells in the stellar photosphere. The idea that convective turnover in red supergiants might take place on extremely large spatial scales had been mentioned in the early 1970's (Stothers & Leung 1971; Stothers 1972) as a possible explanation for their long-term (5–15 year) photometric periodicity. A subsequent analysis of the scale of solar-like supergranulation expected on red supergiants led Schwarzschild (1975) to predict that on smaller scales between 10 and 100 supergranules might be expected at the stellar surface, with turnover times between several months to a year. Numerical modelling of stellar convection (see, for example, Antia, Chitre & Narasimha (1984)) has confirmed these earlier predictions, albeit for lower mass giants ($\sim 1\mathrm{M}_\odot$) than discussed here, and has identified features with temperature excesses of between 300 and 400 K and with lifetimes ranging from 30 to 300 days as being most likely.

The sizes and characteristic timescales of the surface features reported here are too small and rapid to correspond to Stothers' giant cells, but are, however, in remarkable agreement with models for red supergiant supergranulation. Although our images contain no explicit depth information, the fact that the hotspots had similar fractional fluxes and positions both in and out of the TiO band at 710 nm is consistent with a mechanism operating close to the stellar surface, as would be expected in this type of model. In comparison, models invoking changes in the outer cooler regions of the stellar envelope would be expected to lead to hotspots preferentially enhanced at wavelengths corresponding to molecular species. Furthermore, the observed fluxes of the surface features relative to the disc flux agree well with model predictions, and can explain both the magnitude and timescale of the residual irregular photometric variability of the sample stars about their more regular cycles.

Strong circumstantial evidence for localized hotspots on the surfaces of late-type giants has, in the past, come mainly from analyses of polarization observations (see, for example, Hayes 1984; Schwarz & Clarke 1984; Clarke & Brooks 1985; Doherty 1986; Holenstein 1993). Despite the wide range of mechanisms proposed, all of them involve symmetry breaking so as to allow a net polarization to appear in the integrated starlight. The observations presented here suggest that we are seeing these asymmetric features and their effects directly, and that further progress will be possible by correlating the properties of the hotspots with simultaneously collected polarimetric data. For example, the spot fluxes and locations could be used to distinguish between competing physical models for the time-variable net polarization seen in this class of star. Somewhat surprisingly, interferometric observations of Betelgeuse in late 1995 have shown no evidence for any strong asymmetries in the stellar brightness distribution (Baldwin & Burns, private communication) and so it will be interesting to see if this epoch corresponds to a minimum in the measured polarization of the stellar emission.

One issue we have ignored thus far concerns the relationship between surface activity and the extensive mass loss inferred for the target stars (see, for example, Jura & Kleinmann 1990). Using the limits on the sizes and evolution times we have established, we can obtain a rudimentary estimate for the characteristic vertical velocity associated with the surface features. If we assume a distance of 200 pc for Betelgeuse (Jura & Kleinmann 1990) and a typical angular diameter of 44 mas, then a hotspot occupying $\sim 5\%$ of the surface area will have a linear scale of ~ 2 AU. The analysis of Schwarzschild (1975) suggests a depth for the corresponding convective supergranule some 3 times smaller than this, so that timescales of between 3 and 9 months correspond to velocities in the range 5–10 $\mathrm{km\,sec^{-1}}$. These velocities are large when compared to the typical photospheric sound speeds in red supergiants of a few $\mathrm{km\,sec^{-1}}$ (Smith et al. 1989), and even constitute a considerable fraction of the escape velocity ($\sim 40\mathrm{km\,sec^{-1}}$, assuming a mass for α Ori of 10 $\mathrm{M}_\odot$).

If indeed these figures do characterise the velocity of material at the stellar surface then the hotspots could both shock and eject portions of the atmosphere, and thereby provide the primary mechanism initiating mass-loss. This potential for disturbing the stellar atmosphere also implies that the localized brightness enhancements we have detected most likely represent the coupled effects arising from temperature inhomogeneities and their reaction on the stellar atmosphere. Observations of the circumstellar material surrounding late-type supergiants are often suggestive of anisotropy (see, for example, Danchi et al. 1994 and references therein), further strengthening the link between mass loss and photospheric irregularities. An implication of this model is that vigorous surface activity, as indicated by the presence of large hotspot complexes, would be expected to be followed by gradual dimming and reddening of the stellar flux as gas ejected from the stellar surface condensed to dust in regions further from the star. Hopefully, future multi-wavelength monitoring campaigns will be able to test this hypothesis.

4 CONCLUSIONS

We have presented new optical interferometric observations of three M-supergiants (α Ori, α Her, and α Sco) obtained using NRM techniques at the 4.2 m WHT. All of the stars showed evidence for surface activity between 1992 January and 1993 December during which time they were repeatedly observed at a number of wavelengths. At all epochs, the stellar brightness distributions could be described by the superposition of a circularly symmetric disc and a small number of unresolved hotspots contributing between 5 and 20% of the total flux. The ubiquity of these features, together with their numbers, evolution timescales, and colours, are all consistent with a convective origin. We argue that the hotspots are the signatures of the supergranulation cells first described by Schwarzschild (1975), and inferred on the basis of the rapid and irregular photometric and polarimetric variability seen in this class of star. Furthermore, despite our small sample size, it seems likely that this type of surface activity is very common amongst stars of this spectral type and luminosity class. Although diffraction-limited imaging has provided the most direct view of these features, a range of high-precision observations, for example astrometric measurements, will be affected by this phenomenon and will need to be interpreted appropriately.

ACKNOWLEDGMENTS

Financial support from the Royal Society (CAH), the Cambridge Commonwealth Trust and the Cambridge Philosophical Society (PGT) are gratefully acknowledged. We are also grateful to the many members of our group, without whom the observations reported here would not have been possible. The William Herschel Telescope is operated on the island of La Palma by the Royal Greenwich Observatory in the Spanish Observatorio del Roque de los Muchachos of the Instituto de Astrofísica de Canarias.

REFERENCES

Antia H.M., Chitre S.M., Narasimha D., 1984, ApJ, 282, 574
Baliunas S., Dupree A.K., 1982, ApJ, 252, 668
Bedding T.R., Robertson J.G., Marson R.G., 1994, A&A, 290, 240
Belvedere G., Chiuderi C., Paterno L., 1982, A&A, 105, 133
Bessell M.S.,Brett J.M., Scholz M., Wood P.R., 1989, A&A, 213, 209
Buscher D.F., Haniff C.A., Baldwin J.E., Warner P.J., 1990, MNRAS, 245, 7p
Cheng A.Y.S., Hege E.K., Hubbard E.N., Goldberg L., Strittmatter P.A., Cocke W.J., 1986, ApJ, 309, 737
Clarke D., Brooks A., 1985 MNRAS, 212, 211
Danchi W.C., Bester M., Degiacomi C.G., Greenhill L.J., Townes C.H., 1994, AJ, 107, 1469
Doherty L.R., 1986, ApJL, 307, 261
Dupree A.K., Baliunas S.L., Hartmann L., Nassiopoulos G.E., Guinan E.F., Sonneborn G., 1987, ApJL, 317, L85
Dupree A.K., Baliunas S.L., Hartmann L., Guinan E.F., Sonneborn G., 1990, in Cacciari C., Clementini, G., eds, Confrontation between stellar pulsation and evolution. Astron. Soc. Pac., San Francisco, p. 468
Dyck H.M., Benson J.A., van Belle G.T., Ridgway, S.T., 1996, AJ, 111, 1705
Evans D.S., 1957, AJ., 62, 83
Gilliland R.L., Dupree A.K., 1996, ApJ, 463, L29
Haniff C.A., Mackay C.D., Titterington D.J., Sivia D., Baldwin J.E., Warner P.J., 1987, Nat, 328, 694
Hayes D.P., 1984, ApJS, 55, 179
Holenstein B.D., 1993, PASP, 105, 322
Jura M., Kleinmann S.G., 1990, ApJS, 73, 769
Karovska M., Nisenson P., Noyes R., 1986, ApJ, 308, 260
Krisciunas K., 1994, Inf. Bull. Variable Stars, 4028
McAlister H.A., Hartkopf W.I., Sowell J.R., Dombrowski E.G., Franz O.G., 1989, AJ, 97, 510
Maggio A., Vaiani G.S., Haisch B.M., Stern R.A., Bookbinder J., Harnden F.R., Jr, Rosner R., 1990, ApJ, 348, 253
Manduca A., Bell R.A., Gustafsson B., 1977, A&A, 61, 809
Pearson T.J., Readhead A.C.S., 1984, ARA&A, 22, 97
Richichi A., Lisi F., 1990, A&A, 230, 355
Scholz M., Takeda, Y., 1987, A&A, 186, 200
Schwarz H.E., Clarke D., 1984, A&A, 132, 370
Schwarzschild M., 1975, ApJ, 195, 137
Smith M.A., Patten B.M., Goldberg L., 1989, AJ, 98, 2233
Smith M.A., Teays T.J., Taylor L.L., Wasatonic R., Guinan E.F., Baliunas S., 1995, in Stobie R.S., Whitelock P.A., eds, Proc IAU Colloq. 155, Astrophysical applications of stellar pulsation. Astron. Soc. Pac., San Francisco, p. 403
Stothers R., Leung K.C., 1971, A&A, 10, 290
Stothers R., 1972, A&A, 18, 325
Vaiana G.S. et al., 1981, ApJ, 245, 163
Wilson R.W., 1992, PhD thesis, Univ. Cambridge
Wilson R.W., Baldwin J.E., Buscher D.F., Warner P.J., 1992, MNRAS, 257, 369